

MatGPTQ: Accurate and Efficient Post-Training Matryoshka Quantization

Maximilian Kleinegger ^{*12} Elvir Crnčević ³ Dan Alistarh ²³

Abstract

Matryoshka Quantization (MatQuant) is a recent quantization approach showing that a single integer-quantized model can be served across multiple precisions, by slicing the most significant bits (MSB) at inference time. This enables a single checkpoint to cover a wide range of memory and latency budgets, but renders quantization much more challenging. In particular, the initial MatQuant relies on expensive quantization-aware training (QAT) variants, rather than fast one-shot post training quantization (PTQ), and lacks open-source and kernel support. We address all of these limitations by introducing *Post-Training Matryoshka Quantization* (MatGPTQ), a new PTQ pipeline that produces a single parent model jointly optimized for multiple target precisions in one-shot, based on a small calibration set. MatGPTQ casts Matryoshka quantization as a multi-precision objective with bit-slicing and cross-bit error compensation, resulting in an algorithm that produces a multi-bit-width, “sliceable” model in a single pass. We also incorporate a new budget-aware search for heterogeneous per-layer bit-widths and provide efficient kernels that implement slicing and mixed-precision execution. Across standard LLMs and benchmarks, MatGPTQ preserves high-bit accuracy while substantially improving performance at low-bit-width settings. Overall, we establish a new state of the art for Matryoshka-style *post-training* quantization and make single-checkpoint, multi-precision deployment open and practical. Code is available at <https://github.com/IST-DASLab/MatGPTQ>.

1. Introduction

Quantization is currently the most practical way to shrink the memory and bandwidth costs of large language models (LLMs): by mapping full-precision weights to low-bit representations, one can enable single-GPU or edge deployment, while mostly retaining model accuracy. One-shot, post-training quantization (PTQ) is attractive for its low cost and strong accuracy in the 3-4 bit regime (Frantar et al., 2022; Kurtic et al., 2024), whereas optimization-based methods such as QAT and block-wise, gradient-calibrated PTQ (e.g., OmniQuant (Shao et al., 2023)) achieve higher accuracy, but at the expense of extra computational cost.

The recent *Matryoshka Quantization* (MatQuant) work of Nair et al. (2025) provided a fresh approach to model compression by turning integer bit representations into a *nested representation*: a single “parent” model quantized at the highest precision can be *sliced* (via most-significant bit (MSB) extraction) at runtime to yield lower-bit models, enabling sliced variants of a single parent checkpoint to serve many deployment budgets. The MatQuant paper demonstrates single-model, multi-precision training and shows that slicing supports bit-width interpolation, e.g., 6- and 3-bit from an 8-bit parent. Further, the paper suggested the possibility of Mix-and-Match trade-offs between cost and accuracy, by non-uniform per-layer slicing. Follow-up work such as Any-Precision LLM (Park et al., 2024) explored an orthogonal *upscaling* route for multi-scale PTQ, by starting from a low-bit model, and progressively adding bits for increasing accuracy.

Despite this promise, the initial MatQuant evaluations are confined to *finetuning-based* quantization methods, such as QAT and block-wise QAT (OmniQuant), as opposed to the cheaper and more popular one-shot PTQ methods, such as GPTQ (Frantar et al., 2022; Shao et al., 2023; Nair et al., 2025). MatQuant’s description fixes the trained target set to the canonical triplet of $\{8,4,2\}$ bit-widths (with interpolation to $\{6,3\}$), rather than offering a general multi-target PTQ recipe and implementation for arbitrary bit-widths (Nair et al., 2025). While heterogeneous quantization is discussed, the paper does not explore how to search for bit-widths in order to balance accuracy and deployment costs. Further, no code nor kernels were released at the time of writing.

^{*}Work done during an internship at ISTA, ¹Vienna University of Technology, Vienna, Austria ²Institute of Science & Technology Austria (ISTA), Vienna, Austria ³Red Hat AI, Boston, USA. Correspondence to: Dan Alistarh <dan.alistarh@ist.ac.at>.

Contributions. We address these gaps with *Post-Training Matryoshka Quantization* (MatGPTQ), a PTQ framework that optimizes a *single* parent model jointly for a user-specified set of bit-widths R (e.g., $\{2, 3, 4, 6, 8\}$ bits per parameter). Algorithmically, we (i) cast Matryoshka training as a new type of *multi-precision* GPTQ objective with cross-bit error sharing and MSB slicing; (ii) provide open and efficient compression and GPU kernel implementations supporting *more than two* nested precisions, including integer 2–8 bits with bit-width interpolation; and (iii) integrate a principled evolutionary search for *heterogeneous* per-layer bit-width assignment under fixed memory budgets (Sieberling et al., 2025). We release kernels, packing, and a vLLM (Kwon et al., 2023) integration required for end-to-end deployment.

Experimental results. We evaluate MatGPTQ across a suite of modern LLMs, including LLaMA 3.1 8B, Qwen3 (8B/14B), and Phi-3-Medium. Our results demonstrate that MatGPTQ successfully produces a single nested model that performs similarly or better relative to independently-trained, non-nested GPTQ baselines. Crucially, MatGPTQ preserves accuracy at higher bit-widths (4–8 bits, within 0.7% of baseline) while achieving gains in the challenging low-bit regime, showing a 1.34% average improvement at 3 bits, relative to the uniform quantization baseline. Overall, the method matches or outperforms the QAT approach of Nair et al. (2025), and also exhibits strong “interpolation” capabilities, by maintaining accuracy when slicing models at intermediate bit-widths (e.g., 6-bit) for which the model did not optimize explicitly.

Furthermore, we validate the integration of evolutionary search for heterogeneous, non-uniform per-layer quantization. This “Mix-and-Match” approach yields configurations that are often Pareto-superior to standard uniform PTQ, achieving comparable or higher accuracy at lower average bit-widths, even down to 2.5 bits. Finally, we benchmark our optimized CUDA kernels, confirming significant end-to-end latency improvements. For instance, 3-bit inference on LLaMA 3.1 8B achieves nearly a 3x end-to-end speedup compared to FP16 execution on NVIDIA GPUs, demonstrating the practical viability of deploying sliceable models.

All in all, MatGPTQ shows that efficient, and open-source post-training Matryoshka quantization is eminently viable, lowering the barrier of entry for multi-precision deployment.

2. Background and Related Work

Quantization is often applied as a *post-training* (PTQ) step, in one-shot to already trained models. We focus on such one-shot PTQ methods in this paper, by contrast to more expensive quantization-aware training (QAT). For PTQ, one can differentiate between *data-free* approaches, which use sim-

pler round-to-nearest (RTN) projections (Dettmers, 2016; Badri & Shaji, 2023), but tend to drop accuracy even at 4-bits per parameter, and *data-aware* approaches such as GPTQ (Frantar et al., 2022) or AWQ (Lin et al., 2024), which utilize a calibration set that is passed through the model during quantization. Specifically, a common approach in PTQ is to quantize each linear layer ℓ with weights W_ℓ , in linear order, to produce the quantized weights Q_ℓ . Please see Section 3 for an overview of the GPTQ algorithm.

Matryoshka Quantization (MatQuant) (Nair et al., 2025) is a general-purpose multi-scale quantization technique whose objective is to generate “nested” models, in the sense that the higher-bitwidth models “contain” the lower-bitwidth models. More precisely, in MatQuant, for certain bit-widths r , one can slice the most significant r bits out of a c -bit model, with $0 < r < c$, to obtain a valid model, which can be done via the following shift operation:

$$S(q^c, r) = \text{clamp}\left(\left\lfloor \frac{q^c}{2^{c-r}} \right\rfloor, 0, 2^r - 1\right) \cdot 2^{c-r}. \quad (1)$$

They then define their objective function, which minimizes over θ , representing the set of model and auxiliary parameters being optimized. The loss function $\mathcal{L}(\cdot)$ is evaluated for a fixed target set of bit-widths $R = r_1, r_2, \dots, r_K$, under the quantization method $Q(\cdot)$ and forward pass $F(\cdot)$, and is calculated as:

$$\min \frac{1}{N} \sum_{i \in [N]} \sum_{r \in R} \lambda_r \cdot \mathcal{L}(F(S(Q(\theta, c), r), x'_i, y'_i)) \quad (2)$$

Furthermore, they define $y'_i = y_i$ and $x'_i = x_i$ for QAT, and $y'_i = F_\ell(W_F^\ell, X_i^\ell)$ and $x'_i = X_i^\ell$ for OmniQuant. The parameter λ_r is used to weight the importance of individual bit-widths, allowing the optimization to emphasize different bit-widths accordingly.

Nair et al. (2025) produce a single “main” model that can be deployed to various devices with different memory limitations, where the largest model that fits the memory budget is “sliced” from the main model at runtime. For quantization, the authors show results both with standard QAT, adapted to a regularized MatQuant objective, and with a block-wise QAT variant based on the OmniQuant method (Shao et al., 2023). Moreover, the authors suggest the possibility of a Mix-and-Match variant, supporting non-uniform layer-wise quantization. However, their work has some limitations including: (i) focus on quantizing the Feed-Forward-Network (FFN) layers, only considering Attention Weights in the context of QAT, (ii) basic strategies and no practical results for the Mix-and-match approach, (iii) neither their proof-of-concept implementation nor models are publicly available and (iv) no kernels are available.

In this context, our work presents the first post-training (PTQ) and open-source variant of MatQuant, supporting

multiple bit-widths and enabling quantization across a range from 3 to 8 bits using PTQ. It demonstrates performance that is either superior, or on par (within noise) compared to standard, non-nested instances of PTQ. Furthermore, in a direct comparison it outperforms MatQuant’s OmniQuant implementation. Additionally, we are the first to provide CUDA kernels that enable inference speedups and memory savings, as well as support for heterogeneous quantization.

Further Related Work. *Any-Precision LLM* (Park et al., 2024) introduces an *up-scaling* method built on top of SqueezeLLM’s clustered, non-uniform quantization. Yet, their method always loads the full n -bit model into memory and performs dynamic slicing during inference, instead of deploying only the target bit-width. Furthermore, deploying a heterogenous model (mix-and-match) is restricted, as they rely on a fixed quantization layout. The paper states that upscaling cannot be applied to GPTQ or AWQ. Further, D²MoE (Wang et al., 2025) nests multiple bit-widths into one model by adapting GPTQ specifically for Mixture-of-Experts (MoE) layers. Their approach is based on an asymmetric GPTQ version, where each incremental bit-width has its own scale. This is limited by the tested bit-widths of 2, 3 and 4 and being specifically designed for MoE-layers.

Non-Uniform Quantization, where layers can be quantized to different bit-widths based on their sensitivity relative to the model output, presents a different way of exploring the accuracy-compression trade-off (He et al., 2018; Frantar & Alistarh, 2022; Yin et al., 2024). However, choosing non-uniform per-layer bit-widths to maximize accuracy while minimizing model size is not an easy problem, as the corresponding optimization landscape is known to be highly irregular (Sieberling et al., 2025). To solve this for MatQuant, we adapt the state-of-the-art algorithm for this problem, called EvoPress (Sieberling et al., 2025), to the nested compression format.

3. Matryoshka GPTQ

The original MatQuant presented two alternative compression strategies: 1) full-model QAT or 2) block-wise QAT (via OmniQuant (Shao et al., 2023)) focusing only on compressing FFN layers. We investigate full model compression, via a more efficient post-training (one-shot) PTQ method. Specifically, we adapt the classic GPTQ algorithm to the MatQuant objective in Equation 2.

3.1. Adapting GPTQ to the MatQuant Objective

Recall that our objective is, for each layer ℓ in our model, to map its weights W_ℓ to a set of lower bit-widths $R = \{r_1, r_2, \dots, r_K\}$ under consideration, all below a master bit-width c , which is the highest bit-width we are optimizing for, and is the base for our scale and zero-offset. Furthermore,

$$R = \{r_1, \dots, r_K\} \subset \{2, \dots, c\} \text{ with } c \in R.$$

In the context of the GPTQ problem in Equation 5, we start by adapting the method for obtaining quantized weights Q_ℓ^c for a layer ℓ under the master bit-width c , to optimize for target bit-widths while considering the importance of each individual bit-width r :

$$\arg \min_{Q_\ell^c} \sum_{r \in R} \lambda_r \cdot (W_\ell - S(Q_\ell^c, r))^2. \quad (3)$$

Furthermore, we expand Equation 2 to optimize for multiple target bit-widths, taking into account the original layer-wise formulation and the corresponding calibration data X_ℓ :

$$\arg \min_{Q_\ell^c} \sum_{r \in R} \|S(Q_\ell^c, r)X_\ell - W_\ell X_\ell\|. \quad (4)$$

Slicing. Focusing on the slicing operation formalized in Equation 1, recall that we slice the r -most significant bits (MSB) from the base quantized weights. Moreover, we also follow the idea of Nair et al. (2025) to “push” values into higher buckets, thereby allowing more information to be stored. This prevents rounding quantized weights down to zero, as the r most significant bits to be sliced could otherwise be zero. When extracting an r -bit model, we first extract the $(r-1)$ most significant bits and set the r^{th} bit to 1 if the $(r+1)^{th}$ bit is set, and to 0 otherwise. Equally important is the use of $\text{clamp}(\cdot)$ to ensure the validity of usable bits. Furthermore, a right shift of the same magnitude of the slice allows to see the slicing operation as basically being an approximation of the c -bit model.

Cross-bit-width weighting. Furthermore, we use the parameters λ to give different importances to bit-widths: for instance, we may wish to give lower bit-widths higher importance. We present a thorough ablation of this parameter, suggesting that uniform weighting is close to optimal.

3.2. The MatGPTQ Algorithm

In this section, we present a GPTQ-style algorithm, which we call MatGPTQ, whose goal is to produce a nested MatQuant model by performing a single layer-by-layer pass over the original model.

GPTQ Overview. GPTQ solves the data-aware layer-wise quantization problem in Equation 5 w.r.t. W_ℓ and the calibration data X_ℓ :

$$\text{argmin}_{Q_\ell} \|Q_\ell X_\ell - W_\ell X_\ell\|^2. \quad (5)$$

Specifically, GPTQ attempts to approximate the greedy-optimal solution to this problem by leveraging information about the layer-wise Hessian matrix $X_\ell X_\ell^\top$, which is in this case dependent only on the input, and can therefore be

shared among the matrix rows as long as weight updates are performed in a particular order.

Specifically, given a layer’s weights W_ℓ and calibration inputs X_ℓ , GPTQ quantizes weights across *all rows* in the same fixed order, compensating for the quantization error by updating the “free” unquantized weights. Quantizing across all rows simultaneously enables GPTQ to share the Hessian information, used to compute error updates, among rows at each step. Thus, the inverse Hessian must be updated only once per column (d_{col} times) with complexity $O(\max\{d_{\text{row}} \cdot d_{\text{col}}, d_{\text{col}}^3\})$. The native algorithmic blueprint can be found in the Appendix and is illustrated in Algorithm 2.

From GPTQ to MatGPTQ. Algorithm 2 (Appendix) outlines the key differences between the original GPTQ algorithm and the MatGPTQ algorithm, outlined below:

1. First, for the grid choice, scale and zero-offset are calculated following the master bit-width c . Specifically, in our implementation, weights are quantized together in contiguous groups, and we approximate MSE-optimal scaling factors for each group via grid search.
2. The quantized projection for layer ℓ , Q_ℓ^c , is not obtained by rounding to the nearest value on the quantization grid. Instead, we use the objective specified in Equation 2 to obtain Q_ℓ^c considering the cross-bit-width weighting.

The exact approach is described in Algorithm 1. It works by first generating all possible quantized values in the range $[0, Q_{\text{max}}]$ for each individual weight. For every target bit-width, these candidates are then dequantized using the respective scale and zero-offset as previously described. The reconstruction error is computed per weight and accumulated across all candidates, weighted by their respective importance. This results in the total error for each potential quantized value of every weight. Finally, for each weight, the quantized value with the lowest total error is selected. The advantage of this approach lies in its high degree of vectorization and parallelization, making it extremely efficient. Runtime concerns are discussed in the Appendix A.1.

3. Error propagation must be performed across multiple bit-widths at a time. We solve this as follows: Instead of propagating only the single error that one bit-width would produce, as in native GPTQ, we average the errors produced by all target bit-widths and propagate that through the remaining weights. Note that we do not use λ_r to scale these errors. Even though we generate the quantized weights using cross-bit-width weighting, we still propagate the error from each target bit-width equally throughout the network.

Algorithm 1 Generate \mathbf{Q}^c given weight matrix \mathbf{W} , target bit-widths R , and weights λ_R

```

 $Q_{\text{max}} \leftarrow 2^c - 1$ 
 $\mathbf{Q}^c \leftarrow \mathbf{0}_{(Q_{\text{max}}+1) \times d_{\text{row}} \times d_{\text{col}}}$ 
 $\mathbf{Q}^c \leftarrow \text{initQ}(\mathbf{Q}^c, Q_{\text{max}})$   $\triangleright$  assigns  $0, \dots, Q_{\text{max}}$  across the first dimension
 $\mathbf{E} \leftarrow \mathbf{0}_{(Q_{\text{max}}+1) \times d_{\text{row}} \times d_{\text{col}}}$ 
for  $r \in R$  do
     $\mathbf{E} \leftarrow \mathbf{E} + \lambda_r (\mathbf{W} - \text{dequant}(S(\mathbf{Q}^c, r)))^2$ 
end for
 $\mathbf{Q}^c \leftarrow Q_{\arg \min_q \mathbf{E}_q}$   $\triangleright$  elementwise selection of minimal-error quantized weights

```

Extending MatQuant to floating-point representations still remains challenging, as slicing the MSB increases values exponentially rather than linearly, since the exponent is encoded within the bit representation and contributes to the value as a power of two (Nair et al., 2025). Therefore, this remains a future direction to explore.

3.3. Searching for Non-Uniform Sliced Configurations

Given a MatQuant model and a memory budget, a natural optimization is to identify a set of non-uniform bit-widths (one per layer) which minimize model size while maximizing model accuracy. This defines the model that will be instantiated at runtime; finding an “optimal” such model is a variant of classic non-uniform quantization problem (He et al., 2018; Frantar & Alistarh, 2022).

The EvoPress Approach. Currently, the state-of-the-art for this problem for LLMs is the EvoPress $(1 + \lambda)$ -elitist evolutionary algorithm (Sieberling et al., 2025). This algorithm works as follows. We start a generation with a single “parent” model; in each generation, λ “children” (further referred to as offspring) models are generated and evaluated, and the best one, if improving upon the parent, is selected as a new parent for the next generation.

For quantization, we take the MatGPTQ model and stitch the sliced layers together to form an offspring. To generate a new offspring, EvoPress introduces a *level-switch* mutation, meaning that for each layer with decreased bit-width, another of equal size will be increased. This approach allows to maintain the memory constraints, and to make small steps towards an optimal solution. Second, the authors employ a *multi step selection*, whereby, in the beginning, each offspring will be evaluated only on a small subset of calibration data. Then, the best sub-set of offspring are evaluated on significantly more calibration data; in the last step, just a few will be evaluated on the full data, in order to select the best offspring.

Searching over the Matryoshka Space. In the case of

Matryoshka models, the above approach works as follows. The original level-switch mutation uses a fixed step size to control by how many bits equally sized layers are increased or decreased. Since this value is static, having a non-uniform search space, as is the case for us, leads to a disadvantage. We address this as follows: we track remaining available bits after decreasing the bit-width of one layer, and search for a valid bit-width configuration that fits within the available bit budget. Thus, we can increase or decrease multiple layers to find a valid configuration and may retry multiple times if no valid setup is found initially.

4. Fast Matryoshka Kernels

In the following, we describe the design and implementation of an efficient CUDA kernel with support for 2-4 “nested” bit-widths, optimized for low-batch matrix-matrix multiplication latency. We target the Ampere architecture, but the same approach can be extended to Hopper. (Similarly to how the Marlin kernel (Frantar et al., 2024) was extended to Machete (Wilkinson, 2024) for Hopper.) In particular, the quantized weights W_Q will be de-quantized on-the-fly. We denote their de-quantized form as W_D , along with the input X , also stored in FP16. Then, the kernel computes the multiplication $\mathbf{Y} = \mathbf{X}W_D$, with the accumulator being stored in FP32.

The implementation has two primary goals. First, we utilize the NVIDIA TensorCores. For this, we choose the `mma.m16n8k16` instruction as the workhorse of the implementation. The low-batch setting implies that the outer dimension of \mathbf{X} is small. Therefore, we opt to transpose the computation and deviate slightly from the `torch.nn.Linear` convention to execute:

$$\mathbf{Y} = (W_D^T \mathbf{X}^T)^T. \quad (6)$$

Second, we implement a mechanism of batched conversion from quantized weights into their 16-bit form by packing the weights into groups of 4 bits using the conversion techniques presented in Kim et al. (2022). In the 4-bit regime, we can directly apply their 4-bit conversion intrinsics (Kim et al., 2022). However, to support batched conversion in the full 2-4 bit range at no additional storage cost, we split the storage buffer into 3 distinct buffers. The first 64-bit buffer stores the lower 2-bit values of the number, while the rest store the corresponding 1-bit values packed into two 32-bit buffers.

Because these values need to be unpacked on-the-fly during computation, in an offline pre-processing step, we reorder the weights informed by both the dequantization scheme and the register reordering imposed by the TensorCore.

Finally, we implement an additional variant of the kernel which utilizes SIMT cores for low batch inference when the

outer dimension of the input is below 8. We continue to use the TensorCore-informed reordering scheme to avoid maintaining two separate model instances, even though SIMT cores do not require a specific weight ordering.

5. Experiments

5.1. General Setup

Models & Data. We experiment with LLaMA 3.1-8B Instruct and non-Instruct (Base) variants (Dubey et al., 2024), as well as Qwen3 8B and 14B models (Yang et al., 2025), and Phi-3-Medium (Abdin et al., 2024). We choose these models to provide a broad selection of both instruct-tuned and non-instruct models, across common deployment sizes on commodity hardware.

To establish a point of comparison, we use models quantized using the native GPTQ algorithm for the respective bit-width under evaluation. Details about the hyperparameters can be found in the Appendix B.

Pytorch & Huggingface Transformers. Since delivering an open-source version of our work was a major goal, we built our code on top of the widely used PyTorch-based Hugging Face framework (Wolf et al., 2019).

To account for potential performance overhead introduced by using Hugging Face, we conduct not only end-to-end inference measurements but also isolated benchmarks for matrix operations of our GPU kernels. This allows us to evaluate the standalone performance of our kernels and demonstrate the potential improvements achievable in a more optimized inference environment, such as the vLLM engine (Kwon et al., 2023).

Evaluation Datasets. Following established methodology (Frantar et al., 2022), we evaluate all the models based on perplexity and average zero-shot accuracy across a collection of tasks. We use WikiText’s test set (Merity et al., 2016) for evaluating the perplexity and ARC Challenge tasks (ARC-c, ARC-e) (Clark et al., 2018), HellaSwag (Zellers et al., 2019), PIQA (Bisk et al., 2020) and Winogrande (Sakaguchi et al., 2021) for zero-shot task evaluation.

Hardware. All experiments were performed on an NVIDIA RTX A6000 using CUDA 12.4.

5.2. Accuracy Evaluations for MatGPTQ

We now focus on examining the accuracy of *MatGPTQ* based on the different models and benchmarks we prior specified. We consider FFN and Attention layers, compared to MatQuant only quantizing FFN layers using OmniQuant (Nair et al., 2025).

For our experiments, we choose the bit-widths $R = \{3, 4, 8\}$, with the master bit-width $c = 8$ as the optimiza-

Table 1. MatGPTQ across Llama3.1-8B non-Instruct, Instruct, Qwen3 8B non-Instruct, Instruct, 14B Instruct and Phi3-Medium models. MatGPTQ performs on par with the baseline for bitwidths 3, 4, 8 with exception on individual bitwidths for specific models. Even the 6-bit models obtained through interpolation from MatGPTQ perform comparably to the explicitly trained baselines. Additional improvements by incorporating EvoPress are included by MatGPTQ-EP. Task Avg. is average accuracy on the evaluation tasks (\uparrow) while PPL (perplexity) is computed on Wikitext2 test-set (\downarrow).

	LLama3.1-8B		LLama3.1-8B-Instruct		Qwen3-8B-Base		Qwen3-8B		Qwen3-14B		Phi3-Medium		
	PPL	Task Avg	PPL	Task Avg	PPL	Task Avg	PPL	Task Avg	PPL	Task Avg	PPL	Task Avg	
16	6.27	74.52	7.23	74.00	7.01	73.55	9.73	71.54	8.64	74.95	4.32	77.04	
8	GPTQ	6.27	74.49	7.23	73.96	7.01	73.50	9.73	71.61	8.64	74.97	4.32	76.96
	MatGPTQ	6.46	73.07	7.46	73.35	7.29	73.27	9.79	71.86	9.00	75.02	4.54	74.48
4	GPTQ	6.75	72.16	7.84	72.65	7.36	73.62	10.48	70.49	8.88	74.52	4.76	76.47
	MatGPTQ	6.89	72.43	7.82	72.62	7.94	72.74	9.98	70.79	9.05	73.89	4.80	75.97
3	GPTQ	11.31	61.78	11.85	64.57	8.90	69.06	11.58	67.06	10.16	71.02	6.15	72.11
	MatGPTQ	9.14	66.39	10.16	67.56	10.16	67.78	12.74	65.43	10.63	70.95	6.21	72.26
	MatGPTQ-EP	8.73	67.79	9.79	68.58	9.41	67.44	12.35	64.67	9.88	71.01	6.21	72.75
6	GPTQ	6.27	74.05	7.23	73.28	7.04	73.65	9.71	71.42	8.66	74.80	4.34	77.00
	MatGPTQ	6.57	72.74	7.55	73.11	7.49	73.02	9.87	71.35	9.09	74.96	5.06	73.66

tion target. We focus on these bit-widths because the 3–4 bit regime is particularly relevant for low-cost deployment while already achieving high recovery of model performance. (The default GPTQ implementation fails to produce accurate models at any groupsize for our experiments.)

Main Results. We evaluated the uniform configuration $\lambda_3 = \lambda_4 = \lambda_8 = 1$ against the native GPTQ implementation for the respective bit-widths. This balanced configuration demonstrated the best overall performance across all bit-widths with an average maximum percentual deviation from the best results of only 0.25% and at most 0.64%. On average, this outperforms all other configurations, as visible in Table 12.

Table 1 shows that, on average across all models and bit-widths (3, 4, and 8), MatGPTQ stays within a 0.08% relative difference over native GPTQ implementation in terms of average task performance. Considering the individual bit-widths, we observe that 3-bit quantization improves average task performance by 1.34% relative to native GPTQ. This can be explained, by the regularization in the quantization grid search (Algorithm 1), which optimizes for multiple bit-widths and therefore prevents overfitting to calibration data for a single bit-width. Whereas the 4-bit and 8-bit configurations exhibit slightly lower performance by 0.33% and 0.65%, respectively, which falls within the expected noise. This showcases the strong performance of MatGPTQ, producing nested models that perform on par with natively GPTQ-quantized models.

Generally, the method also works well across different models (non-Instruct vs Instruct), as all show similar behavior with in terms of accuracy drops. The only exceptions are the 3-bit variant of Qwen3-8B and Qwen3-8B-Base, which performs worse compared to the native GPTQ. Interestingly, Phi3-Medium 6- and 8-bit variant shows the strongest degra-

dation compared to its 4-bit variant. This can be addressed by using the 4-bit model, as it outperforms the other bit-widths while improving efficiency. Further, this suggests that the first 4 bits encode the necessary information and additional bits add noise.

Interpolation. As mentioned in (Nair et al., 2025), the MatQuant framework shows good performance, regarding interpolation of bit-widths, which are not directly optimized for. Since, we offer CUDA kernel support for 2, 3, 4, 6 and 8 bit, we are also interested in being able to use a 6-bit model. We can see in Table 1 that the 6-bit MatGPTQ on average performs 0.67% lower than the native GPTQ baseline. This is worse than the bit-widths we optimized for, but still can be considered usable. Also showcasing great interpolation performance across the models, except for Phi3-Medium, where prior reasoning and solution can be applied to the same problem.

5.3. Comparison with the original MatQuant

A comparison to the MatQuant framework is rather hard, since neither source code or models are publicly available. Furthermore, while the authors provided hyperparameters for fine-tuning, they omitted those for evaluation, making the reproduction of results even more challenging. However, we managed to implement MatQuant for OmniQuant, hereafter referred to as MatQuant, and produce models that fall within their reported performance. For a fair comparison, we only quantized the FFN layers for both Mistral 7B (Jiang et al., 2023) and Gemma2 9B (Team et al., 2024) as reported by them using MatQuant and MatGPTQ. We used symmetric quantization for both methods an optimized for bit-widths $R = 3, 4, 8$. Further details about the hyperparameters can be found in the Appendix B.

In Table 2, we can see that MatGPTQ outperforms

Table 2. Comparison of Task Average (\uparrow) between MatGPTQ and MatQuant, for Mistral 7B and Gemma2 9B (FFN-only). MatGPTQ achieves higher results compared to MatQuant for all optimized and interpolated bit-wtdhs.

	Gemma2 9B		Mistral 7B	
	MatQuant	MatGPTQ	MatQuant	MatGPTQ
16	78.23		74.56	
8	77.78	78.18	74.37	74.65
4	77.20	77.93	73.92	74.24
3	75.45	75.47	71.85	72.19
6	77.76	78.12	74.35	74.79

MatQuant for each optimized and interpolated bit-wtdh. This can be observed even though OmniQuant potentially outperforms GPTQ in low bit regimes (Shao et al., 2023). However by default OmniQuant uses asymmetric quantization and therefore performs worse when applied with symmetric quantization. A full comparison when quantizing FFN+Attention is not possible against the MatQuant implementation, as Nair et al. (2025) do not provide any code. However, since MatGPTQ is able to perform FFN+Attention quantization and still performing close to native GPTQ, outperforming MatQuant for FFN only and being a simpler and more efficient method than OmniQuant, we can conclude that MatGPTQ improves upon MatQuant.

5.4. The impact of loss weights λ_r

The introduction of the weighting factor λ_r resulted in introducing the need for a search over potential importance weightings, as no configuration seemed superior (Nair et al., 2025). We used the weights $\{0.1, 0.5, 1\}$ and generated promising candidates. We compare a uniform weighting approach against two configurations that highly value the lowest bit-wtdhs and equally value the remaining bit-wtdhs at different magnitudes, one configuration that decreases the weighting for higher bit-wtdhs, and one configuration that equally values the lowest two bit-wtdhs while minimizing the importance of the highest bit-wtdh. As already mentioned the uniform approach has turned out to be the best with an average maximum percentual deviation from the best results of only 0.24% and at most 0.64%.

Therefore, we conclude that a more extensive search can lead to slightly better results, although at the additional cost of training and evaluating many more models. If it is known that a specific bit-regime needs to achieve the best performance, a specific weighting should be considered. However, if the goal is to maintain strong performance across all bit-regimes, uniform weighting remains a good choice. Evaluation results and further details about the ablation study can be found in the Appendix E.

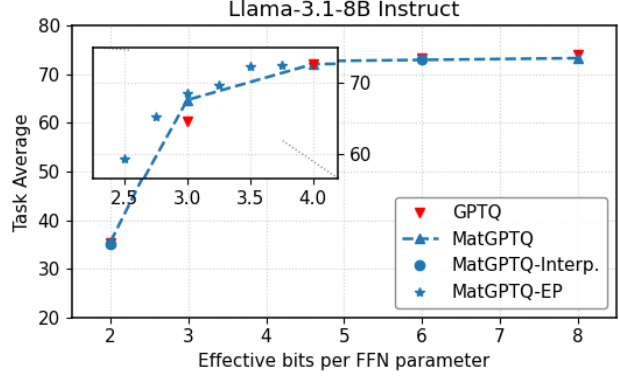


Figure 1. Task average performance of Llama3.1-8B-Instruct quantized using MatGPTQ optimizing for 3, 4 and 8 bits. The results demonstrate that even under extreme compression, MatGPTQ maintains strong performance, with models between 2.5 and 4 bits achieving near-baseline accuracy for optimized bit-wtdhs and even exceeding it for interpolated bit-wtdhs.

5.5. Mix-and-Match Models

Since potential losses in the low bit regime can occur due to quantization to multiple bit-wtdhs, we leverage non-uniformity to improve the accuracy of all 3-bit models to either achieve baseline performance or even exceed it and to generate multiple Llama3.1-8B-Instruct models between 2- and 4-bit to demonstrate their capabilities. This allows us to use this pipeline to even produce usable models for extremely resource-constrained environments: even though 2-bit models themselves have very low accuracy, slicing only a fraction of the layers to this bit-width can still provide good accuracy.

Search Space. We restrict the search space to $\{2, 3, 4, 6, 8\}$ bits, in order to be able to fully leverage our CUDA kernels. We use the search approach described in Section 3.3.

Results. First, Table 1 shows that our non-uniform variant, referred to as MatGPTQ-EP, outperforms both the baseline and the uniform MatGPTQ models across all evaluated architectures. This demonstrates the effectiveness of our method, as it eliminates the losses observed with uniform configurations, allowing us to produce models that perform equally well or even surpass their baselines.

In Figure 1, we can see the performance of EvoPress in the low-bit regimes. Starting from 2.5 bits, we already obtain a usable model, with low accuracy loss. Furthermore, every non-optimized bit-wtdh exceeds its theoretical interpolated counterpart, indicated by the dotted line. Using EvoPress, we also manage to surpass the GPTQ-optimized 3-bit model. Also notably, the interpolated 6-bit model aligns almost perfectly with the theoretical line. Those results are especially interesting as they suggest that our MatGPTQ model is Pareto-superior to the pre-trained model quantized

via GPTQ to an equivalent bit-width, as it achieves comparable or higher accuracy at consistently lower bit-widths. Thus, our method offers a more favorable trade-off between performance and computational cost.

Negative Result: Inference-Time bit-width Allocation. Having multiple nested models allows to investigate if it would make sense to *dynamically route different tokens to different bit-widths*, while maintaining certain constraints to improve accuracy of the model. To assess this, we generated all possible configurations within a transformer block for bit-widths 2, 3, and 4 targeting an average bit-width of 3 and compared the MSE for individual tokens. We found that, in most cases, one single *static* configuration consistently outperforms the others. This negative result suggests that such assignments and routing should be explicitly performed at training-time in order to be effective. Further details are in Appendix C.

5.6. CUDA Kernel Performance

We benchmark the kernel speed-ups for weight matrices of size 2048x2048, 4096x4096, 8192x8192 and 16384x16384 while varying the input size. We use `torch.matmul` as a baseline point of comparison. We transition from a SIMT kernel into a TensorCore-based kernel at batch size 8, owing to the size of the inner dimension of the `mma` instruction. All the configurations utilize 128 as the group size. Our kernels achieve speedups between 3x and 5.6x in the memory-bound regime. The peak speed-up is achieved during 2-bit single batch multiplication, owing to the memory-bound regime in that setting. Further details and visualizations can be found in Appendix H.

At higher batch size, the kernel switches to a compute-bound regime and we exhibit slowdowns at around batch size 32 and 64, depending on the bit-width configuration.

5.7. End-to-End Experiments

We run a forward pass of Llama3.1-8B-Instruct with a single token and measure the end-to-end latency while varying the model bit-width utilizing `torch.compile` under `reduce-overhead` and `full-graph` settings during end-to-end runs. The benchmark runs 16 warm-up single-token forward passes. Following that, we do another 16 runs, out of which we report the minimum and the median run in Table 3. The speed-up over the 16-bit version naturally diminishes as bit-widths increase. In the near-lossless regime (3-4 bits), our kernels achieve end-to-end speedups of 2.58-2.9 \times .

Deployment. For practical deployment, we integrated our kernels and format in vLLM (Kwon et al., 2023) and achieved similar speedups. Details are found in the Appendix H.

Table 3. Latency Comparison (ms and tokens/s) for Llama-3.1-8B-Instruct at different Quantization Bit-Widths.

bit-width	Median Latency	Tokens/s	Rel. Speedup
2	7.24	138.0	3.25 \times
3	8.03	124.4	2.93 \times
4	9.13	109.3	2.58 \times
16	23.53	42.5	1.00 \times

6. Discussion & Limitations

In this work, we introduced MatGPTQ, the first practical and efficient framework for Post-Training Matryoshka Quantization (PTQ). By adapting the GPTQ algorithm to optimize a single model jointly for multiple target precisions, MatGPTQ enables “sliceable” quantization in a one-shot manner. The primary advantage of MatGPTQ is deployment flexibility. A single quantized checkpoint can be obtained fast, based on limited calibration data, and can be adapted at runtime to meet diverse memory and latency budgets across various hardware without the overhead of storing and maintaining multiple models. Our extensive evaluation demonstrates that this flexibility comes at virtually no cost to accuracy relative to the GPTQ baseline. We further enhanced MatGPTQ by integrating a budget-aware evolutionary search (EvoPress) to identify optimal heterogeneous per-layer bit-widths. This “Mix-and-Match” approach (MatGPTQ-EP) is effective, yielding configurations that are Pareto-superior to standard PTQ. On the negative side, we showed that routing different tokens to different bit-widths based on sensitivity does not improve accuracy.

In addition, we provided the first open-source implementation for Matryoshka quantization, built on the Hugging Face framework, along with efficient CUDA kernels supporting slicing and mixed-precision execution.

Limitations and Future Work. Our experiments focused on a limited range, and integer quantization; achieving high accuracy in the ultra-low-bit regime remains challenging with the current GPTQ algorithm at standard group sizes. In future work, we will explore integrating Matryoshka objectives with quantization methods better suited for ultra-low precisions, as well as floating-point quantization. Furthermore, while our CUDA kernels provide efficient inference on the NVIDIA Ampere architecture, expanding support to newer GPU architectures (e.g., Hopper, Blackwell) and integrating these kernels into high-throughput serving frameworks like vLLM would be an important future step to enable broader adoption.

Impact Statement

This paper presents work whose goal is to advance the field of Machine Learning. There are many potential societal

consequences of our work, none which we feel must be specifically highlighted here.

References

- Abdin, M., Jacobs, S. A., Awan, A. A., Aneja, J., Awadallah, A., Awadalla, H., Bach, N., Bahree, A., Bakhtiari, A., Behl, H., Benhaim, A., Bilenko, M., Bjorck, J., Bubeck, S., Cai, M., Mendes, C. C. T., Chen, W., Chaudhary, V., Chopra, P., Giorno, A. D., de Rosa, G., Dixon, M., Eldan, R., Iter, D., Garg, A., Goswami, A., Gunasekar, S., Haider, E., Hao, J., Hewett, R. J., Huynh, J., Javaheripi, M., Jin, X., Kauffmann, P., Karampatziakis, N., Kim, D., Khademi, M., Kurilenko, L., Lee, J. R., Lee, Y. T., Li, Y., Liang, C., Liu, W., Lin, E., Lin, Z., Madan, P., Mitra, A., Modi, H., Nguyen, A., Norick, B., Patra, B., Perez-Becker, D., Portet, T., Pryzant, R., Qin, H., Radmilac, M., Rosset, C., Roy, S., Ruwase, O., Saarikivi, O., Saied, A., Salim, A., Santacroce, M., Shah, S., Shang, N., Sharma, H., Song, X., Tanaka, M., Wang, X., Ward, R., Wang, G., Witte, P., Wyatt, M., Xu, C., Xu, J., Yadav, S., Yang, F., Yang, Z., Yu, D., Zhang, C., Zhang, C., Zhang, J., Zhang, L. L., Zhang, Y., Zhang, Y., Zhang, Y., and Zhou, X. Phi-3 technical report: A highly capable language model locally on your phone, 2024.
- Badri, H. and Shaji, A. Half-quadratic quantization of large machine learning models, November 2023. URL https://mobiusml.github.io/hqq_blog/.
- Bisk, Y., Zellers, R., LeBras, R., Gao, J., and Choi, Y. PIQA: reasoning about physical commonsense in natural language. In *The Thirty-Fourth AAAI Conference on Artificial Intelligence, AAAI 2020, The Thirty-Second Innovative Applications of Artificial Intelligence Conference, IAAI 2020, The Tenth AAAI Symposium on Educational Advances in Artificial Intelligence, EAAI 2020, New York, NY, USA, February 7-12, 2020*, pp. 7432–7439. AAAI Press, 2020. URL <https://ojs.aaai.org/index.php/AAAI/article/view/6239>.
- Clark, P., Cowhey, I., Etzioni, O., Khot, T., Sabharwal, A., Schoenick, C., and Tafjord, O. Think you have solved question answering? try arc, the ai2 reasoning challenge. *arXiv preprint arXiv:1803.05457*, 2018.
- Dettmers, T. 8-bit approximations for parallelism in deep learning. *International Conference on Learning Representations (ICLR)*, 2016.
- Dubey, A., Jauhri, A., Pandey, A., Kadian, A., and et al. The Llama 3 herd of models, 2024. URL <https://arxiv.org/abs/2407.21783>.
- Frantar, E. and Alistarh, D. SPDY: Accurate pruning with speedup guarantees. In *International Conference on Machine Learning (ICML)*, 2022.
- Frantar, E., Ashkboos, S., Hoefer, T., and Alistarh, D. GPTQ: Accurate post-training quantization for generative pre-trained transformers. *arXiv preprint arXiv:2210.17323*, 2022.
- Frantar, E., Castro, R. L., Chen, J., Hoefer, T., and Alistarh, D. Marlin: Mixed-precision auto-regressive parallel inference on large language models. *arXiv preprint arXiv:2408.11743*, 2024.
- He, Y., Lin, J., Liu, Z., Wang, H., Li, L.-J., and Han, S. AMC: AutoML for model compression and acceleration on mobile devices. In *European Conference on Computer Vision (ECCV)*, 2018.
- Jiang, A. Q., Sablayrolles, A., Mensch, A., Bamford, C., Chaplot, D. S., Casas, D. d. l., Bressand, F., Lengyel, G., Lample, G., Saulnier, L., et al. Mistral 7b. *arXiv preprint arXiv:2310.06825*, 2023.
- Kim, Y. J., Henry, R., Fahim, R., and Awadalla, H. H. Who says elephants can't run: Bringing large scale moe models into cloud scale production, 2022. URL <https://arxiv.org/abs/2211.10017>.
- Kurtic, E., Marques, A., Pandit, S., Kurtz, M., and Alistarh, D. "give me bf16 or give me death"? accuracy-performance trade-offs in llm quantization. *arXiv preprint arXiv:2411.02355*, 2024.
- Kwon, W., Li, Z., Zhuang, S., Sheng, Y., Zheng, L., Yu, C. H., Gonzalez, J., Zhang, H., and Stoica, I. Efficient memory management for large language model serving with pagedattention. In *Proceedings of the 29th Symposium on Operating Systems Principles*, pp. 611–626, 2023.
- Lin, J., Tang, J., Tang, H., Yang, S., Chen, W.-M., Wang, W.-C., Xiao, G., Dang, X., Gan, C., and Han, S. Awq: Activation-aware weight quantization for llm compression and acceleration. In *Proceedings of the Learning on Systems (MLSys) Conference*, 2024.
- Merity, S., Xiong, C., Bradbury, J., and Socher, R. Pointer sentinel mixture models. *arXiv preprint arXiv:1609.07843*, 2016.
- Nair, P., Datta, P., Dean, J., Jain, P., and Kusupati, A. Matryoshka quantization, 2025. URL <https://arxiv.org/abs/2502.06786>.
- Park, Y., Hyun, J., Cho, S., Sim, B., and Lee, J. W. Any-precision llm: Low-cost deployment of multiple, different-sized llms. *arXiv preprint arXiv:2402.10517*, 2024.
- Penedo, G., Kydlíček, H., allal, L. B., Lozhkov, A., Mitchell, M., Raffel, C., Werra, L. V., and Wolf, T. The fineweb

- datasets: Decanting the web for the finest text data at scale, 2024. URL <https://arxiv.org/abs/2406.17557>.
- Sakaguchi, K., Bras, R. L., Bhagavatula, C., and Choi, Y. Winogrande: An adversarial winograd schema challenge at scale. *Communications of the ACM*, 64(9):99–106, 2021.
- Shao, W., Chen, M., Zhang, Z., Xu, P., Zhao, L., Li, Z., Zhang, K., Gao, P., Qiao, Y., and Luo, P. Omnipoint: Omnidirectionally calibrated quantization for large language models. *arXiv preprint arXiv:2308.13137*, 2023.
- Sieberling, O., Kuznedelev, D., Kurtic, E., and Alistarh, D. Evopress: Accurate dynamic model compression via evolutionary search, 2025. URL <https://arxiv.org/abs/2410.14649>.
- Team, G., Riviere, M., Pathak, S., Sessa, P. G., Hardin, C., Bhupatiraju, S., Hussenot, L., Mesnard, T., Shahriari, B., Ramé, A., Ferret, J., Liu, P., Tafti, P., Friesen, A., Casbon, M., Ramos, S., Kumar, R., Lan, C. L., Jerome, S., Tsitsulin, A., Vieillard, N., Stanczyk, P., Girgin, S., Momchev, N., Hoffman, M., Thakoor, S., Grill, J.-B., Neyshabur, B., Bachem, O., Walton, A., Severyn, A., Parrish, A., Ahmad, A., Hutchison, A., Abdagic, A., Carl, A., Shen, A., Brock, A., Coenen, A., Laforge, A., Paterson, A., Bastian, B., Piot, B., Wu, B., Royal, B., Chen, C., Kumar, C., Perry, C., Welty, C., Choquette-Choo, C. A., Sinopalnikov, D., Weinberger, D., Vijaykumar, D., Rogozińska, D., Herbison, D., Bandy, E., Wang, E., Noland, E., Moreira, E., Senter, E., Eltyshev, E., Visin, F., Rasskin, G., Wei, G., Cameron, G., Martins, G., Hashemi, H., Klimczak-Plucińska, H., Batra, H., Dhand, H., Nardini, I., Mein, J., Zhou, J., Svensson, J., Stanway, J., Chan, J., Zhou, J. P., Carrasqueira, J., Iljazi, J., Becker, J., Fernandez, J., van Amersfoort, J., Gordon, J., Lipschultz, J., Newlan, J., yeong Ji, J., Mohamed, K., Badola, K., Black, K., Milligan, K., McDonell, K., Nguyen, K., Sodhia, K., Greene, K., Sjoesund, L. L., Usui, L., Sifre, L., Heuermann, L., Lago, L., McNealus, L., Soares, L. B., Kilpatrick, L., Dixon, L., Martins, L., Reid, M., Singh, M., Iverson, M., Görner, M., Velloso, M., Wirth, M., Davidow, M., Miller, M., Rahtz, M., Watson, M., Risdal, M., Kazemi, M., Moynihan, M., Zhang, M., Kahng, M., Park, M., Rahman, M., Khatwani, M., Dao, N., Bardoliwalla, N., Devanathan, N., Dumai, N., Chauhan, N., Wahltinez, O., Botarda, P., Barnes, P., Barham, P., Michel, P., Jin, P., Georgiev, P., Culliton, P., Kuppala, P., Comanescu, R., Merhej, R., Jana, R., Rokni, R. A., Agarwal, R., Mullins, R., Saadat, S., Carthy, S. M., Cogan, S., Perrin, S., Arnold, S. M. R., Krause, S., Dai, S., Garg, S., Sheth, S., Ronstrom, S., Chan, S., Jordan, T., Yu, T., Eccles, T., Hennigan, T., Kociský, T., Doshi, T., Jain, V., Yadav, V., Meshram, V., Dharmadhikari, V., Barkley, W., Wei, W., Ye, W., Han, W., Kwon, W., Xu, X., Shen, Z., Gong, Z., Wei, Z., Cotruta, V., Kirk, P., Rao, A., Giang, M., Peran, L., Warkentin, T., Collins, E., Barral, J., Ghahramani, Z., Hadsell, R., Sculley, D., Banks, J., Dragan, A., Petrov, S., Vinyals, O., Dean, J., Hassabis, D., Kavukcuoglu, K., Farabet, C., Buchatskaya, E., Borgeaud, S., Fiedel, N., Joulin, A., Kenealy, K., Dadashi, R., and Andreev, A. Gemma 2: Improving open language models at a practical size, 2024. URL <https://arxiv.org/abs/2408.00118>.
- Wang, H., Zhou, Q., Hong, Z., and Guo, S. D²moe: Dual routing and dynamic scheduling for efficient on-device moe-based llm serving. *arXiv preprint arXiv:2504.15299*, 2025.
- Wilkinson, L. Introducing machete, a mixed-input gemm kernel optimized for nvidia hopper gpus. Red Hat Developer, October 2024. URL <https://developers.redhat.com/articles/2024/10/14/introducing-machete-mixed-input-gemm-kernel>. Accessed: 2025-10-30.
- Wolf, T., Debut, L., Sanh, V., Chaumond, J., Delangue, C., Moi, A., Cistac, P., Rault, T., Louf, R., Funtowicz, M., et al. Huggingface’s transformers: State-of-the-art natural language processing. *arXiv preprint arXiv:1910.03771*, 2019.
- Yang, A., Li, A., Yang, B., Zhang, B., Hui, B., Zheng, B., Yu, B., Gao, C., Huang, C., Lv, C., Zheng, C., Liu, D., Zhou, F., Huang, F., Hu, F., Ge, H., Wei, H., Lin, H., Tang, J., Yang, J., Tu, J., Zhang, J., Yang, J., Yang, J., Zhou, J., Zhou, J., Lin, J., Dang, K., Bao, K., Yang, K., Yu, L., Deng, L., Li, M., Xue, M., Li, M., Zhang, P., Wang, P., Zhu, Q., Men, R., Gao, R., Liu, S., Luo, S., Li, T., Tang, T., Yin, W., Ren, X., Wang, X., Zhang, X., Ren, X., Fan, Y., Su, Y., Zhang, Y., Zhang, Y., Wan, Y., Liu, Y., Wang, Z., Cui, Z., Zhang, Z., Zhou, Z., and Qiu, Z. Qwen3 technical report, 2025. URL <https://arxiv.org/abs/2505.09388>.
- Yin, L., Wu, Y., Zhang, Z., Hsieh, C.-Y., Wang, Y., Jia, Y., Li, G., Jaiswal, A., Pechenizkiy, M., Liang, Y., Bendersky, M., Wang, Z., and Liu, S. Outlier weighed layerwise sparsity (owl): A missing secret sauce for pruning llms to high sparsity, 2024.
- Zellers, R., Holtzman, A., Bisk, Y., Farhadi, A., and Choi, Y. Hellaswag: Can a machine really finish your sentence? *arXiv preprint arXiv:1905.07830*, 2019.

A. MatGPTQ Implementation Details

Algorithm 2 outlines the native GPTQ algorithm, including the key differences between the native GPTQ algorithm and the MatGPTQ algorithm in blue. In Algorithm 2 $\text{quant}_{\text{MatGPTQ}}(\cdot)$ refers to Algorithm 1.

Algorithm 2 Quantize \mathbf{W} given inverse Hessian $\mathbf{H}^{-1} = (2\mathbf{X}\mathbf{X}^\top + \lambda\mathbf{I})^{-1}$, block size B and master bitwidth c , optimizing for lower bitwidths R with weights λ_R

$\mathbf{Q} \leftarrow \mathbf{0}_{d_{\text{row}} \times d_{\text{col}}}$	▷ quantized output
$\mathbf{E} \leftarrow \mathbf{0}_{d_{\text{row}} \times B}$	▷ block quantization errors
$\mathbf{H}^{-1} \leftarrow \text{Cholesky}(\mathbf{H}^{-1})^\top$	▷ hessian inverse information
for $i = 0, B, 2B, \dots$ until $i < d_{\text{col}}$ do	
for $j = i, \dots, i + B - 1$ do	
$\mathbf{Q}_{:,j} \leftarrow \text{quant}_{\text{MatGPTQ}}(\mathbf{W}_{:,j}, R, \lambda_R)$	▷ quantize column
$\mathbf{E}_{:,j-i} \leftarrow \frac{1}{ R } \sum_{r \in R} (\mathbf{W}_{:,j} - S(\mathbf{Q}^c_{:,j}, r)) / [\mathbf{H}^{-1}]_{jj}$	▷ quantization error
$\mathbf{W}_{:,i:i+B-1} \leftarrow \mathbf{W}_{:,i:i+B-1} - \mathbf{E}_{:,j-i} \mathbf{H}_{j,i:i+B-1}^{-1}$	▷ update weights in block
end for	
$\mathbf{W}_{:,i+B:d_{\text{col}}-1} \leftarrow \mathbf{W}_{:,i+B:d_{\text{col}}-1} - \mathbf{E} \mathbf{H}_{i:i+B-1,i+B:d_{\text{col}}-1}^{-1}$	▷ update all remaining weights
end for	

A.1. Performance considerations for $\text{quant}_{\text{MatGPTQ}}(\cdot)$

Table 4. Per-layer quantization runtime comparison between native GPTQ and MatGPTQ. We report the overall layer runtime, average quantization runtime, and the percentage of total layer execution time spent in quantization.

	Native GPTQ			MatGPTQ		
	Overall Runtime	Avg. Runtime Alg. 1	% of layer time	Overall Runtime	Avg. Runtime Alg. 1	% of layer time
self.attn.q.proj	1.40 (4.20)	0.000121	35.24	3.59	0.000602	68.72
self.attn.k.proj	1.41 (4.22)	0.000121	35.37	3.58	0.000602	68.97
self.attn.v.proj	1.40 (4.23)	0.000121	35.31	3.58	0.000603	68.99
self.attn.o.proj	1.40 (4.21)	0.000121	35.36	3.56	0.000600	68.97
mlp.gate.proj	1.42 (4.24)	0.000122	35.08	6.18	0.000595	39.43
mlp.up.proj	1.42 (4.23)	0.000122	35.10	6.18	0.000596	39.50
mlp.down.proj	5.37 (15.36)	0.000121	32.34	12.90	0.000599	66.50

With Algorithm 1 we want to optimize the quantization grid for multiple bitwidths. We decided to take a simple brutforce approach instead of relying on any heuristics, as this approach is still highly vectorizable and the resulting overhead appeared acceptable considering our target of optimizing for multiple bitwidths.

To validate this, we measured execution times while quantizing a Llama-3.1-8B-Instruct model using the native GPTQ implementation and the MatQuant implementation. In Table 4, we observe that on average MatQuant takes 5x longer to quantize the weights. We also see an increase of overall execution time and execution time spent on quantizing the weights. However, if we compare quantizing to multiple bitwidths as indicated by the overall execution times in the brackets for native GPTQ, we can see that MatGPTQ is actually faster for its target. Only the layers `gate_proj` and `gate_proj` take longer and this can be explained by the increased input dimension compared to the other layers.

B. Additional Hyperparameter Details

This section presents the hyperparameters used for the respective methods.

B.1. MatGPTQ and GPTQ

For both the native GPTQ and MatGPTQ, we use the Fineweb-Edu (Penedo et al., 2024) dataset as calibration data. Specifically, we use 2,097,152 tokens, corresponding to 1024 samples with a sequence length of 2048. Furthermore, we use a group size of 128, a dampening factor of 0.01, and symmetric quantization. For completion, we optimized for bitwidths $r = \{3, 4, 8\}$ and used uniform bitwidth weights $\lambda_3 = \lambda_4 = \lambda_8 = 1$.

B.2. MatQuant

For MatQuant (Nair et al., 2025), we followed the specific hyperparameters provided by the authors: for Gemma2 9B we used $\lambda_3 = 1$, $\lambda_4 = 0.1$, and $\lambda_8 = 0.1$, and for Mistral 7B we used $\lambda_3 = 1$, $\lambda_4 = 0.4$, and $\lambda_8 = 0.4$. We used their constant learning rate of 10^{-3} and a batch size of 4. We only differ by using symmetric quantization and optimizing for $r = 3, 4, 8$. Additionally, we apply grouping of size 128 to make the comparison even fairer, even though they never mention anything regarding grouping.

B.3. EvoPress

The hyperparameters for all EvoPress runs can be found in Table 5.

Table 5. Hyperparameters for EvoPress runs.

Hyperparameter	Value
Generations	100
Offspring	64
Survivors (1)	16
Tokens (1)	2048
Survivors (2)	16384
Tokens (2)	4
Survivors (3)	1
Tokens (3)	131072
Fitness Function	KL-Divergence
Calibration Data	Fineweb Edu
Calibration Tokens	524288
Calibration sequence length	2048
Initially generated (if applicable)	10

C. Dynamic Bitwidth Inference

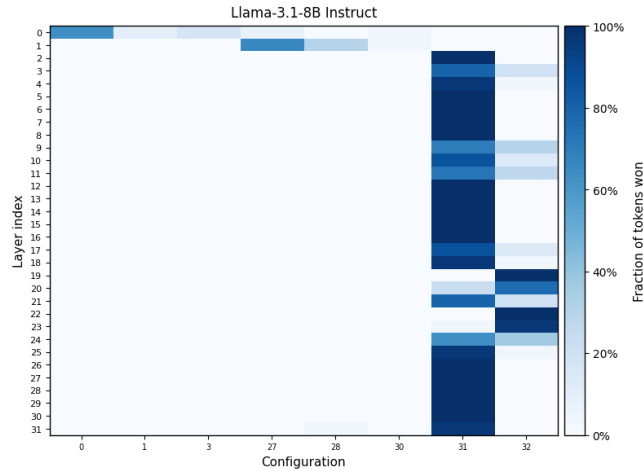


Figure 2. Heatmap of best-performing quantization configurations across transformer blocks of Llama-3.1-8B Instruct. We enumerated all configurations for bitwidths 2, 3 and 4 under an average bitwidth of 3 and measured per-token MSE against the FP16 baseline. Configurations without a single token are omitted. A single static configuration dominates across most blocks, with certain layers showing higher sensitivity.

Since, we wanted to explore the sensitivity of different non-uniform configurations towards single tokens, we generated all possible configurations within a transformer block for bitwidths 2, 3, and 4 targeting an average bitwidth of 3. Then, we measured the MSE for individual tokens compared to the FP16 model for each individual configuration in each transformer

block. We conducted these initial experiments using the Llama 3.1 8B Instruct model to assess whether further investigation was worthwhile. As the results were already quite clear, we limited our study to this model and did not conduct additional experiments. The results can be seen in Figure 2. There, we can see that, in most cases, one single *static* configuration consistently outperforms the others, and certain transformer blocks appear consistently more sensitive. Therefore, this suggests that dynamic token assignment cannot provide significant improvements. This negative result suggests that such assignments and routing should be explicitly performed at training-time in order to be effective. Furthermore, as reported by (Sieberling et al., 2025), we observe higher sensitivity in the early and late layers.

D. Detailed Evaluations for MatGPTQ

Tables 6, 7, 9, 8, 10 and 11 present detailed evaluation results on Llama3.1-8B Instruct, Non-Instruct, Qwen3 8B, Qwen3 8B Base, Qwen3 14B and Phi3-Medium with MatGPTQ.

Table 6. Table presents the evaluation results for MatGPTQ on Llama3.1-8B-Instruct. Average is average accuracy on the evaluation tasks (\uparrow) while PPL (perplexity) is computed on Wikitext2 test-set (\downarrow).

LLama3.1-8B-Instruct								
Bitwidth	Method	PPL	ARC-c	ARC-e	HellaSwag	PIQA	Winogrande	Average
16		7.23	55.89	79.80	79.52	81.34	73.48	74.00
8	GPTQ	7.23	55.80	79.76	79.44	81.07	73.72	73.96
	MatGPTQ	7.46	55.20	78.83	78.39	80.69	73.64	73.35
4	GPTQ	7.84	52.47	79.80	77.75	79.82	73.40	72.65
	MatGPTQ	7.82	52.82	79.84	77.40	80.96	72.06	72.62
3	GPTQ	11.85	42.24	69.53	68.82	75.08	67.17	64.57
	MatGPTQ	10.16	46.25	70.92	72.92	76.44	71.27	67.56
6	GPTQ	7.23	54.27	78.07	79.33	81.12	73.64	73.28
	MatGPTQ	7.55	54.61	78.32	78.32	80.74	73.56	73.11

Table 7. Table presents the evaluation results for MatGPTQ on Llama3.1-8B. Average is average accuracy on the evaluation tasks (\uparrow) while PPL (perplexity) is computed on Wikitext2 test-set (\downarrow).

LLama3.1-8B								
Bitwidth	Method	PPL	ARC-c	ARC-e	HellaSwag	PIQA	Winogrande	Average
16		6.27	54.95	82.53	79.29	81.23	74.59	74.52
8	GPTQ	6.27	55.12	82.62	79.27	80.96	74.51	74.49
	MatGPTQ	6.46	52.90	80.47	78.37	80.85	72.77	73.07
4	GPTQ	6.75	51.37	79.34	77.11	79.60	73.40	72.16
	MatGPTQ	6.89	51.88	78.96	77.36	80.96	73.01	72.43
3	GPTQ	11.31	39.42	64.65	66.28	73.29	65.27	61.78
	MatGPTQ	9.14	44.88	71.55	70.52	75.84	69.14	66.39
6	GPTQ	6.27	54.27	81.44	79.23	80.96	74.35	74.05
	MatGPTQ	6.57	52.13	80.18	77.94	80.85	72.61	72.74

E. Detailed Evaluations for the impact of loss weights λ_R

We compare a uniform weighting approach against two configurations that highly value the lowest bitwidths and equally value the remaining bitwidths at different magnitudes, one configuration that decreases the weighting for higher bitwidths,

Table 8. Table presents the evaluation results for MatGPTQ on Qwen3-8B-Base. Average is average accuracy on the evaluation tasks (\uparrow) while PPL (perplexity) is computed on Wikitext2 test-set (\downarrow).

Qwen3-8B-Base								
Bitwidth	Method	PPL	ARC-c	ARC-e	HellaSwag	PIQA	Winogrande	Average
16		7.01	56.91	80.01	78.65	79.33	72.85	73.55
8	GPTQ	7.01	56.91	79.84	78.61	79.60	72.53	73.50
	MatGPTQ	7.29	56.91	79.17	77.08	79.82	73.40	73.27
4	GPTQ	7.36	57.34	81.44	77.89	79.22	72.22	73.62
	MatGPTQ	7.94	56.66	78.96	77.23	79.43	71.43	72.74
3	GPTQ	8.90	51.79	76.26	73.16	77.64	66.46	69.06
	MatGPTQ	10.16	48.63	74.75	71.25	77.42	66.85	67.78
6	GPTQ	7.04	57.59	80.43	78.54	79.00	72.69	73.65
	MatGPTQ	7.49	55.97	79.46	76.86	80.03	72.77	73.02

Table 9. Table presents the evaluation results for MatGPTQ on Qwen3-8B. Average is average accuracy on the evaluation tasks (\uparrow) while PPL (perplexity) is computed on Wikitext2 test-set (\downarrow).

Qwen3-8B								
Bitwidth	Method	PPL	ARC-c	ARC-e	HellaSwag	PIQA	Winogrande	Average
16		9.73	56.57	80.93	74.94	77.69	67.56	71.54
8	GPTQ	9.73	56.31	80.93	74.94	77.75	68.11	71.61
	MatGPTQ	9.79	56.48	80.72	74.65	77.86	69.61	71.86
4	GPTQ	10.48	54.52	79.42	73.94	76.71	67.88	70.49
	MatGPTQ	9.98	55.29	80.09	74.15	76.39	68.03	70.79
3	GPTQ	11.58	47.53	75.29	70.29	75.79	66.38	67.06
	MatGPTQ	12.74	48.72	72.31	67.18	74.32	64.64	65.43
6	GPTQ	9.71	56.66	80.18	74.77	77.48	68.03	71.42
	MatGPTQ	9.87	55.55	79.76	74.62	77.69	69.14	71.35

and one configuration that equally values the lowest two bitwidths while minimizing the importance of the highest bitwidth. As shown in Table 12, for bitwidths 3, one configuration consistently performs better than the others across most models. However, for bitwidth 4, each model exhibits a distinct best configuration. It is noteworthy that the largest differences appear in the 3-bit regime, while for higher bitwidths, variations are negligible, differing by at most 0.65%, as seen with Llama3.1-8B-Instruct. In contrast, for 3-bit quantization, differences can reach up to 1.93%, also observed for Llama3.1-8B-Instruct.

Tables 13, 14, 15, 16, 17, 18 present detailed evaluation results on the impact of the loss weights λ_R for Llama3.1-8B Instruct, Non-Instruct, Qwen3 8B Base, Qwen3 8B, Qwen3 14B and Phi3-Medium with MatGPTQ.

F. Detailed Evaluations for Mix'n'Match MatGPTQ

Table 19 presents detailed evaluation results on applying Mix'N'Match for Llama3.1-8B Instruct, Non-Instruct, Qwen3 8B, Qwen3 14B and Phi3-Medium with average bitwidth of 3. Table 20 presents detailed evaluation for 2-4 bit Mix'N'Match LLama3.1-8B-Instruct.

Table 10. Table presents the evaluation results for MatGPTQ on Qwen3-14B. Average is average accuracy on the evaluation tasks (\uparrow) while PPL (perplexity) is computed on Wikitext2 test-set (\downarrow).

Qwen3-14B								
Bitwidth	Method	PPL	ARC-c	ARC-e	HellaSwag	PIQA	Winogrande	Average
16	Baseline	8.64	60.24	82.83	78.86	79.82	73.01	74.95
8	GPTQ	8.64	60.32	82.79	78.73	79.87	73.16	74.97
	MatGPTQ	9.00	61.09	82.62	77.41	80.36	73.64	75.02
4	GPTQ	8.88	60.58	82.74	77.97	79.54	71.74	74.52
	MatGPTQ	9.05	58.70	81.73	77.54	79.54	71.90	73.89
3	GPTQ	10.16	54.95	76.89	75.78	78.94	68.51	71.02
	MatGPTQ	10.63	55.12	77.69	75.72	77.53	68.67	70.95
6	GPTQ	8.66	60.41	82.74	78.77	79.87	72.22	74.80
	MatGPTQ	9.09	60.84	82.15	77.64	80.47	73.72	74.96

Table 11. Table presents the evaluation results for MatGPTQ on Phi3-Medium. Average is average accuracy on the evaluation tasks (\uparrow) while PPL (perplexity) is computed on Wikitext2 test-set (\downarrow).

Phi3-Medium								
Bitwidth	Method	PPL	ARC-c	ARC-e	HellaSwag	PIQA	Winogrande	Average
16		4.32	61.52	82.83	83.64	82.86	74.35	77.04
8	GPTQ	4.32	61.35	82.66	83.70	82.75	74.35	76.96
	MatGPTQ	4.54	59.04	76.77	79.40	80.85	76.32	74.48
4	GPTQ	4.76	60.84	82.41	82.72	82.75	73.64	76.47
	MatGPTQ	4.80	60.49	80.51	81.59	82.05	75.22	75.97
3	GPTQ	6.15	54.18	74.75	79.10	80.14	72.38	72.11
	MatGPTQ	6.21	56.14	76.52	77.82	79.92	70.88	72.26
6	GPTQ	4.34	61.35	82.87	83.70	82.75	74.35	77.00
	MatGPTQ	5.06	58.36	74.71	79.43	80.74	74.98	73.64

G. Detailed Evaluations for Comparison of MatGPTQ vs MatQuant (OmniQuant)

The detailed evaluation results used for the comparison of MatGPTQ against MatQuant (OmniQuant) for FFN-only can be found in Tables 21 and 22 for Gemma2 9B and Mistral 7B, respectively.

H. CUDA Kernel Performance Evaluations

We benchmark the kernel speed-ups for weight matrices of size 2048x2048, 4096x4096, 8192x8192 and 16384x16384 while varying the input size. The results can be seen in Figure 3. As already mentioned, our kernels achieve speedups between 3x and 5.6x in the memory-bound regime. The peak speed-up is achieved during 2-bit single batch multiplication, owing to the memory-bound regime in that setting.

Furthermore, we present our end-to-end speedups in vLLM (Kwon et al., 2023) for Llama-3.1-8B-Instruct in Figure 4. We report both latency reductions and throughput improvements. Overall speedups between 1.5x and 3.5x can be achieved in the memory-bound regime.

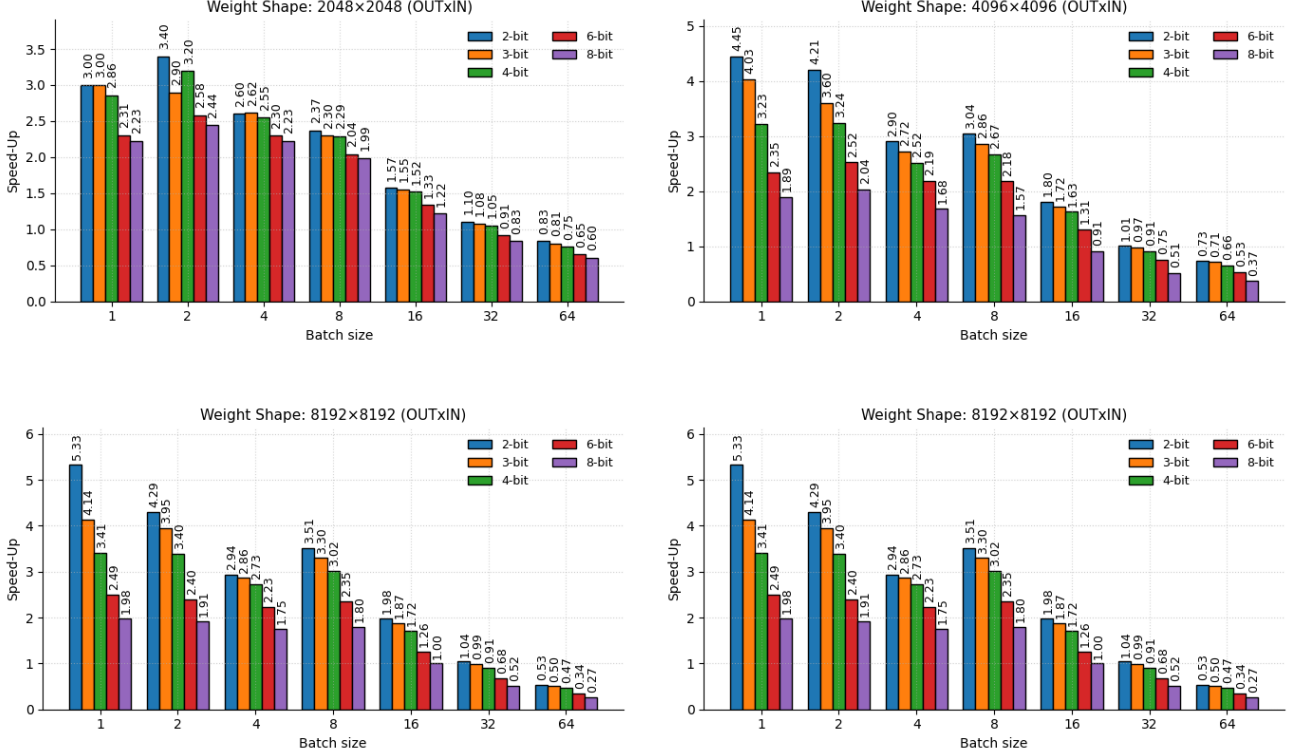


Figure 3. Benchmark results comparison across multiple matrix dimensions with `torch.matmul` as the baseline. Our kernels achieve speedups between 3x and 5.6x in the memory-bound regime.

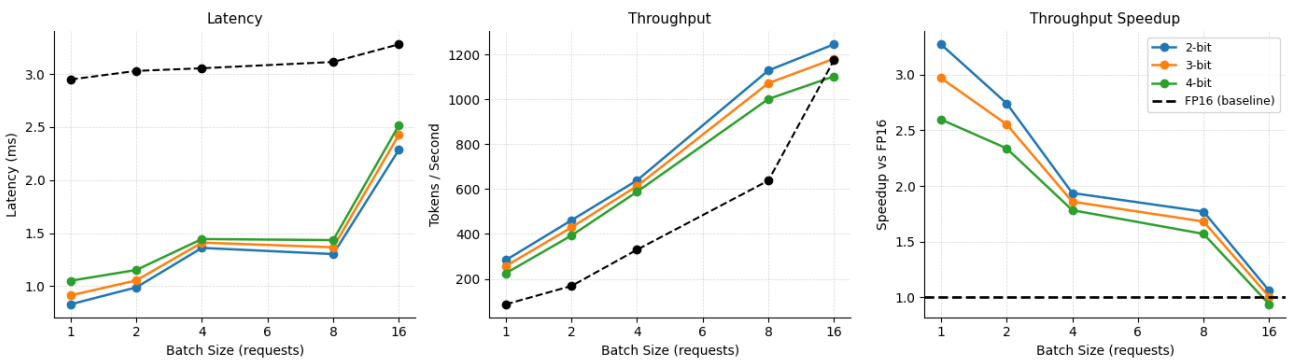


Figure 4. End-to-end speedups in vLLM (Kwon et al., 2023) for Llama-3.1-8B-Instruct. Our kernels achieve speedups between 1.5x and 3.5x in the memory-bound regime. We evaluated on an RTX A6000 using Prompt/Decode 32/128.

Table 12. Evaluation results on Llama3.1-8B non-Instruct, Instruct, Qwen3 8B, 14B and Phi3-Medium models for MatGPTQ using different loss weighting strategies. Task Avg. is average accuracy on the evaluation tasks (\uparrow). Weightings: $(x, y, z) \rightarrow (\lambda_3, \lambda_4, \lambda_8)$

Bitwidth	Weightings	Task Avg					
		LLama3.1-8B	LLama3.1-8B-Instruct	Qwen3-8B-Base	Qwen3-8B	Qwen3-14B	Phi3-Medium
8	(1, 0.1, 0.1)	73.08	73.66	73.20	71.90	74.93	74.43
	(1, 0.5, 0.1)	73.06	73.28	73.28	71.86	74.97	74.66
	(1, 0.5, 0.5)	73.19	73.51	73.26	72.13	75.05	74.40
	(1, 1, 0.1)	73.01	73.39	73.45	72.08	75.00	74.61
	(1, 1, 1)	73.07	73.35	73.27	71.86	75.02	74.48
4	(1, 0.1, 0.1)	72.37	72.39	72.57	70.85	74.12	75.70
	(1, 0.5, 0.1)	72.23	72.63	72.53	70.69	74.25	75.74
	(1, 0.5, 0.5)	72.28	72.68	72.37	70.61	74.01	76.14
	(1, 1, 0.1)	72.05	72.33	72.91	70.92	73.91	75.78
	(1, 1, 1)	72.43	72.62	72.74	70.79	73.89	75.97
3	(1, 0.1, 0.1)	65.72	66.71	67.19	64.31	71.09	71.98
	(1, 0.5, 0.1)	66.23	67.82	66.90	64.41	70.51	71.99
	(1, 0.5, 0.5)	66.63	66.88	67.76	64.33	70.62	71.91
	(1, 1, 0.1)	66.81	67.99	67.37	64.60	70.72	72.24
	(1, 1, 1)	66.39	67.56	67.78	65.43	70.95	72.26

Table 13. Table presents evaluation results for MatGPTQ on Llama-3.1-8B for different λ_R configurations. Average is average accuracy on the evaluation tasks (\uparrow). Weightings: $(x, y, z) \rightarrow (\lambda_3, \lambda_4, \lambda_8)$

Llama-3.1-8B							
Bitwidth	Importance Weights λ_R	ARC-c	ARC-e	HellaSwag	PIQA	Winogrande	Average
8	(1, 0.1, 0.1)	53.41	80.35	78.41	80.85	72.38	73.08
	(1, 0.5, 0.1)	53.16	80.18	78.36	80.90	72.69	73.06
	(1, 0.5, 0.5)	53.16	80.64	78.44	80.85	72.85	73.19
	(1, 1, 0.1)	52.82	79.80	78.34	81.07	73.01	73.01
	(1, 1, 1)	52.90	80.47	78.37	80.85	72.77	73.07
4	(1, 0.1, 0.1)	51.71	78.87	77.15	80.79	73.32	72.37
	(1, 0.5, 0.1)	51.45	78.70	77.26	80.41	73.32	72.23
	(1, 0.5, 0.5)	51.28	79.25	77.38	80.25	73.24	72.28
	(1, 1, 0.1)	50.77	78.37	77.51	80.85	72.77	72.05
	(1, 1, 1)	51.88	78.96	77.36	80.96	73.01	72.43
3	(1, 0.1, 0.1)	43.69	69.28	70.73	75.79	69.14	65.72
	(1, 0.5, 0.1)	43.00	71.46	70.52	76.61	69.53	66.23
	(1, 0.5, 0.5)	44.97	71.46	70.57	76.55	69.61	66.63
	(1, 1, 0.1)	45.39	72.22	70.71	76.44	69.30	66.81
	(1, 1, 1)	44.88	71.55	70.52	75.84	69.14	66.39
6	(1, 0.1, 0.1)	52.99	79.76	78.02	80.69	72.53	72.80
	(1, 0.5, 0.1)	52.47	80.01	77.97	81.12	73.24	72.96
	(1, 0.5, 0.5)	52.90	80.22	78.01	80.63	72.77	72.91
	(1, 1, 0.1)	52.56	79.97	78.13	80.69	72.77	72.82
	(1, 1, 1)	52.13	80.18	77.94	80.85	72.61	72.74

Table 14. Table presents evaluation results for MatGPTQ on Llama-3.1-8B-Instruct for different λ_R configurations. Average is average accuracy on the evaluation tasks (\uparrow). Weightings: $(x, y, z) \rightarrow (\lambda_3, \lambda_4, \lambda_8)$

Llama-3.1-8B-Instruct							
Bitwidth	Importance Weights λ_R	ARC-c	ARC-e	HellaSwag	PIQA	Winogrande	Average
8	(1, 0.1, 0.1)	55.55	79.00	78.42	81.07	74.27	73.66
	(1, 0.5, 0.1)	54.78	79.12	78.27	80.74	73.48	73.28
	(1, 0.5, 0.5)	55.38	78.91	78.29	80.96	74.03	73.51
	(1, 1, 0.1)	55.03	79.21	78.23	81.07	73.40	73.39
	(1, 1, 1)	55.20	78.83	78.39	80.69	73.64	73.35
4	(1, 0.1, 0.1)	52.39	79.21	77.31	80.20	72.85	72.39
	(1, 0.5, 0.1)	52.82	79.92	77.21	80.36	72.85	72.63
	(1, 0.5, 0.5)	53.50	79.67	77.25	80.47	72.53	72.68
	(1, 1, 0.1)	52.13	79.08	77.35	79.98	73.09	72.33
	(1, 1, 1)	52.82	79.84	77.40	80.96	72.06	72.62
3	(1, 0.1, 0.1)	46.33	69.23	73.07	74.65	70.24	66.71
	(1, 0.5, 0.1)	47.53	71.76	72.96	75.95	70.88	67.82
	(1, 0.5, 0.5)	46.16	69.91	72.96	75.90	69.46	66.88
	(1, 1, 0.1)	46.76	72.47	72.87	76.28	71.59	67.99
	(1, 1, 1)	46.25	70.92	72.92	76.44	71.27	67.56
6	(1, 0.1, 0.1)	54.95	78.58	78.47	80.79	73.95	73.35
	(1, 0.5, 0.1)	54.35	78.79	78.28	80.47	72.85	72.95
	(1, 0.5, 0.5)	54.69	78.79	78.36	81.01	73.72	73.31
	(1, 1, 0.1)	54.69	78.20	78.23	81.12	73.88	73.22
	(1, 1, 1)	54.61	78.32	78.32	80.74	73.56	73.11

Table 15. Table presents evaluation results for MatGPTQ on Qwen3-8B-Base for different λ_R configurations. Average is average accuracy on the evaluation tasks (\uparrow). Weightings: $(x, y, z) \rightarrow (\lambda_3, \lambda_4, \lambda_8)$

Qwen3-8B-Base							
Bitwidth	Importance Weights λ_R	ARC-c	ARC-e	HellaSwag	PIQA	Winogrande	Average
8	(1, 0.1, 0.1)	57.00	79.04	76.93	79.82	73.24	73.20
	(1, 0.5, 0.1)	57.17	78.91	77.01	79.76	73.56	73.28
	(1, 0.5, 0.5)	57.00	78.87	76.95	79.87	73.64	73.26
	(1, 1, 0.1)	57.68	79.04	76.83	79.82	73.88	73.45
	(1, 1, 1)	56.91	79.17	77.08	79.82	73.40	73.27
4	(1, 0.1, 0.1)	56.23	78.87	76.96	79.38	71.43	72.57
	(1, 0.5, 0.1)	57.25	79.21	76.65	79.27	70.24	72.53
	(1, 0.5, 0.5)	55.89	79.04	76.77	78.89	71.27	72.37
	(1, 1, 0.1)	56.48	79.46	77.03	79.22	72.38	72.91
	(1, 1, 1)	56.66	78.96	77.23	79.43	71.43	72.74
3	(1, 0.1, 0.1)	47.27	72.98	71.32	76.99	67.40	67.19
	(1, 0.5, 0.1)	46.67	72.64	71.05	76.82	67.32	66.90
	(1, 0.5, 0.5)	49.57	74.37	71.12	77.37	66.38	67.76
	(1, 1, 0.1)	47.35	73.99	70.91	77.26	67.32	67.37
	(1, 1, 1)	48.63	74.75	71.25	77.42	66.85	67.78
6	(1, 0.1, 0.1)	56.48	79.88	76.83	80.20	74.03	73.48
	(1, 0.5, 0.1)	56.23	78.45	77.00	79.76	73.56	73.00
	(1, 0.5, 0.5)	56.74	79.42	77.07	79.60	73.95	73.36
	(1, 1, 0.1)	57.08	79.76	76.80	79.98	73.56	73.43
	(1, 1, 1)	55.97	79.46	76.86	80.03	72.77	73.02

Table 16. Table presents evaluation results for MatGPTQ on Qwen3-8B for different λ_R configurations. Average is average accuracy on the evaluation tasks (\uparrow). Weightings: $(x, y, z) \rightarrow (\lambda_3, \lambda_4, \lambda_8)$

Qwen3-8B							
Bitwidth	Importance Weights λ_R	ARC-c	ARC-e	HellaSwag	PIQA	Winogrande	Average
8	(1, 0.1, 0.1)	56.14	80.77	74.72	77.86	70.01	71.90
	(1, 0.5, 0.1)	56.23	80.93	74.78	77.80	69.53	71.86
	(1, 0.5, 0.5)	57.00	81.02	74.80	77.97	69.85	72.13
	(1, 1, 0.1)	56.40	80.89	74.65	78.07	70.40	72.08
	(1, 1, 1)	56.48	80.72	74.65	77.86	69.61	71.86
4	(1, 0.1, 0.1)	55.46	79.67	74.34	76.61	68.19	70.85
	(1, 0.5, 0.1)	56.40	79.80	74.06	76.17	67.01	70.69
	(1, 0.5, 0.5)	55.20	79.84	73.90	76.39	67.72	70.61
	(1, 1, 0.1)	55.46	80.30	74.14	76.99	67.72	70.92
	(1, 1, 1)	55.29	80.09	74.15	76.39	68.03	70.79
3	(1, 0.1, 0.1)	47.53	69.91	66.71	74.21	63.22	64.31
	(1, 0.5, 0.1)	46.67	71.13	66.95	74.16	63.14	64.41
	(1, 0.5, 0.5)	48.21	70.08	66.77	73.94	62.67	64.33
	(1, 1, 0.1)	47.87	71.55	66.52	73.61	63.46	64.60
	(1, 1, 1)	48.72	72.31	67.18	74.32	64.64	65.43
6	(1, 0.1, 0.1)	56.57	80.22	74.55	77.58	69.30	71.64
	(1, 0.5, 0.1)	56.14	80.18	74.47	77.58	69.53	71.58
	(1, 0.5, 0.5)	56.48	80.35	74.62	77.97	69.14	71.71
	(1, 1, 0.1)	55.72	80.18	74.59	77.80	69.14	71.48
	(1, 1, 1)	55.55	79.76	74.62	77.69	69.14	71.35

Table 17. Table presents evaluation results for MatGPTQ on Qwen3-14B for different λ_R configurations. Average is average accuracy on the evaluation tasks (\uparrow). Weightings: $(x, y, z) \rightarrow (\lambda_3, \lambda_4, \lambda_8)$

Qwen3-14B							
Bitwidth	Importance Weights λ_R	ARC-c	ARC-e	HellaSwag	PIQA	Winogrande	Average
8	(1, 0.1, 0.1)	60.67	82.58	77.43	80.20	73.80	74.93
	(1, 0.5, 0.1)	61.01	82.24	77.44	80.36	73.80	74.97
	(1, 0.5, 0.5)	61.18	82.83	77.24	80.36	73.64	75.05
	(1, 1, 0.1)	61.18	82.58	77.53	80.14	73.56	75.00
	(1, 1, 1)	61.09	82.62	77.41	80.36	73.64	75.02
4	(1, 0.1, 0.1)	59.13	81.99	77.48	79.92	72.06	74.12
	(1, 0.5, 0.1)	58.87	82.58	77.55	79.82	72.45	74.25
	(1, 0.5, 0.5)	58.96	81.90	77.63	79.82	71.74	74.01
	(1, 1, 0.1)	59.22	81.90	77.60	79.82	71.03	73.91
	(1, 1, 1)	58.70	81.73	77.54	79.54	71.90	73.89
3	(1, 0.1, 0.1)	55.20	77.65	75.71	77.97	68.90	71.09
	(1, 0.5, 0.1)	54.35	77.15	75.88	77.20	67.96	70.51
	(1, 0.5, 0.5)	54.01	77.57	75.86	77.31	68.35	70.62
	(1, 1, 0.1)	54.95	76.81	75.81	77.91	68.11	70.72
	(1, 1, 1)	55.12	77.69	75.72	77.53	68.67	70.95
6	(1, 0.1, 0.1)	60.32	82.37	77.49	80.52	73.64	74.87
	(1, 0.5, 0.1)	60.15	82.20	77.49	80.30	74.03	74.84
	(1, 0.5, 0.5)	59.73	81.94	77.50	80.20	73.95	74.67
	(1, 1, 0.1)	60.67	82.24	77.45	80.20	73.72	74.85
	(1, 1, 1)	60.84	82.15	77.64	80.47	73.72	74.96

Table 18. Table presents evaluation results for MatGPTQ on Phi3-Medium for different λ_R configurations. Average is average accuracy on the evaluation tasks (\uparrow). Weightings: $(x, y, z) \rightarrow (\lambda_3, \lambda_4, \lambda_8)$

Phi3-Medium							
Bitwidth	Importance Weights λ_R	ARC-c	ARC-e	HellaSwag	PIQA	Winogrande	Average
8	(1, 0.1, 0.1)	58.87	76.73	79.60	80.79	76.16	74.43
	(1, 0.5, 0.1)	59.39	77.06	79.63	80.58	76.64	74.66
	(1, 0.5, 0.5)	59.13	76.60	79.43	80.69	76.16	74.40
	(1, 1, 0.1)	59.39	76.89	79.66	80.58	76.56	74.61
	(1, 1, 1)	59.04	76.77	79.40	80.85	76.32	74.48
4	(1, 0.1, 0.1)	59.47	79.80	81.82	82.10	75.30	75.70
	(1, 0.5, 0.1)	60.15	80.01	81.44	81.66	75.45	75.74
	(1, 0.5, 0.5)	60.84	81.27	81.60	81.94	75.06	76.14
	(1, 1, 0.1)	60.07	80.30	81.53	81.94	75.06	75.78
	(1, 1, 1)	60.49	80.51	81.59	82.05	75.22	75.97
3	(1, 0.1, 0.1)	55.55	76.05	77.60	79.60	71.11	71.98
	(1, 0.5, 0.1)	56.14	75.38	77.81	79.49	71.11	71.99
	(1, 0.5, 0.5)	55.97	75.34	77.95	79.33	70.96	71.91
	(1, 1, 0.1)	56.57	76.39	77.74	79.16	71.35	72.24
	(1, 1, 1)	56.14	76.52	77.82	79.92	70.88	72.26
6	(1, 0.1, 0.1)	58.28	75.46	79.51	80.36	75.30	73.78
	(1, 0.5, 0.1)	58.11	74.71	79.40	80.52	74.90	73.53
	(1, 0.5, 0.5)	58.53	74.96	79.62	80.25	75.14	73.70
	(1, 1, 0.1)	58.70	75.08	79.55	80.47	74.74	73.71
	(1, 1, 1)	58.36	74.71	79.43	80.74	74.98	73.64

Table 19. Table presents the evaluation results for Mix’N’Match for Llama3.1-8B Non-Instruct, Instruct, Qwen3 8B-Base, Qwen3 8B, Qwen3 14B and Phi3-Medium with average bitwidth of 3. Average is average accuracy on the evaluation tasks (\uparrow) while PPL (perplexity) is computed on Wikitext2 test-set (\downarrow).

MatGPTQ-EP with average bitwidth of 3							
Model	PPL	ARC-c	ARC-e	HellaSwag	PIQA	Winogrande	Average
LLama3.1-8B	8.73	47.27	71.17	72.54	77.04	70.96	67.79
LLama3.1-8B-Instruct	9.79	47.53	71.46	73.53	77.86	72.53	68.58
Qwen3-8B-Base	9.41	48.21	73.02	72.80	77.20	65.98	67.44
Qwen3-8B	12.35	47.53	68.69	68.40	74.27	64.48	64.67
Qwen3-14B	9.88	53.84	78.24	75.37	78.29	69.30	71.01
Phi3-Medium	6.21	56.40	76.52	79.52	80.03	71.27	72.75

Table 20. Table presents the evaluation results for Mix’N’Match for Llama3.1-8B Instruct for various bitwidths between 2 and 4. It is compared to baseline and MatGPTQ uniform models. Average is average accuracy on the evaluation tasks (\uparrow).

Llama-3.1-8B-Instruct							
Bitwidth	Method	ARC-c	ARC-e	HellaSwag	PIQA	Winogrande	Average
2.00	GPTQ	24.74	27.23	26.29	50.05	48.62	35.39
2.00	MatGPTQ	24.83	25.59	26.52	51.69	48.93	35.51
2.50	MatGPTQ EP	36.52	59.05	63.33	73.34	64.25	59.30
2.75	MatGPTQ EP	43.94	66.08	69.72	75.57	71.11	65.28
3.00	GPTQ	42.24	69.53	68.82	75.08	67.17	64.57
3.00	MatGPTQ	46.25	70.92	72.92	76.44	71.27	67.56
3.00	MatGPTQ EP	47.53	71.46	73.53	77.86	72.53	68.58
3.25	MatGPTQ EP	48.81	72.73	75.84	78.02	73.01	69.68
3.50	MatGPTQ EP	53.58	78.20	77.05	79.05	73.48	72.27
3.75	MatGPTQ EP	53.50	78.03	77.09	79.27	74.43	72.46
4.00	GPTQ	52.47	79.80	77.75	79.82	73.40	72.65
4.00	MatGPTQ	52.82	79.84	77.40	80.96	72.06	72.62
4.00	MatGPTQ EP	53.84	78.58	77.60	79.76	73.56	72.67

Table 21. Table presents the evaluation results for MatGPTQ and MatQuant (FFN-only) on Gemma2 9B. Average is average accuracy on the evaluation tasks (\uparrow).

Gemma2 9B							
Bitwidth	Method	ARC-c	ARC-e	HellaSwag	PIQA	Winogrande	Average
16		66.13	87.79	79.98	82.92	74.35	78.23
8	MatQuant	64.25	87.84	78.75	82.70	75.37	77.78
	MatGPTQ	65.44	87.88	79.72	83.35	74.51	78.18
4	MatQuant	63.23	86.87	78.40	82.05	75.45	77.20
	MatGPTQ	64.85	87.79	79.59	82.97	74.43	77.93
3	MatQuant	59.64	84.89	76.46	81.83	74.43	75.45
	MatGPTQ	59.98	85.27	76.91	80.90	74.27	75.47
6	MatQuant	64.25	87.75	78.72	82.81	75.30	77.76
	MatGPTQ	65.53	87.84	79.60	82.97	74.66	78.12

Table 22. Table presents the evaluation results for MatGPTQ and MatQuant (FFN-only) on Mistral 7B. Average is average accuracy on the evaluation tasks (\uparrow).

Mistral 7B							
Bitwidth	Method	ARC-c	ARC-e	HellaSwag	PIQA	Winogrande	Average
16		54.35	79.38	81.15	82.54	75.37	74.56
8	MatQuant	53.67	79.42	81.05	82.64	75.06	74.37
	MatGPTQ	54.44	79.84	80.98	82.32	75.69	74.65
4	MatQuant	54.01	78.41	81.03	81.88	74.27	73.92
	MatGPTQ	53.84	79.34	81.08	82.10	74.82	74.24
3	MatQuant	50.17	77.15	79.13	80.74	72.06	71.85
	MatGPTQ	50.85	77.10	79.33	80.96	72.69	72.19
6	MatQuant	54.27	79.84	81.02	82.26	74.35	74.35
	MatGPTQ	54.78	79.76	81.04	82.54	75.85	74.79